Journal of Power Sources 273 (2015) 14–24

Contents lists available at ScienceDirect

Journal of Power Sources

journal homepage: www.elsevier.com/locate/jpowsour

The Solid Electrolyte Interphase a key parameter of the high performance of Sb in sodium-ion batteries: Comparative X-ray Photoelectron Spectroscopy study of Sb/Na-ion and Sb/Li-ion batteries

Lucille Bodenes [b], Ali Darwiche [a, c], Laure Monconduit [a, c], Hervé Martinez [b, c, *]

[a] ICG-AIME, Bat 15, cc 15-02 Université Montpellier 2, Pl. E. Bataillon, 34095 Montpellier Cedex, France
[b] IPREM-ECP CNRS UMR 5254, Université de Pau, Hélioparc Pau Pyrénées, 2 av. Pierre Angot, 64053 Pau Cedex 9, France
[c] Réseau sur le Stockage Electrochimique de l'Energie (RS2E), CNRS FR3459, 33 Rue Saint Leu, 80039 Amiens Cedex, France

HIGHLIGHTS

- Sb electrodes formulated with CMC or PVdF as a binder cycled versus Li and Na.
- Outstanding performances of antimony electrode vs Na when it is prepared with CMC.
- Electrochemical performances related to the XPS study of SEI composition/thickness.
- Thinner passivation film formed at the Sb electrode when cycled versus Na.
- SEI homogeneously thick on the Sb-CMC electrode, not on the Sb-PVdF electrode.

ARTICLE INFO

Article history:
Received 22 July 2014
Received in revised form
26 August 2014
Accepted 7 September 2014
Available online 16 September 2014

Keywords:
Sodium-ion batteries
Lithium-ion batteries
Antimony
Solid Electrolyte Interphase
X-ray Photoelectron Spectroscopy
Binder

ABSTRACT

To understand the origin of the better performance of Sb electrode i) vs Na than vs Li and ii) formulated with CarboxyMethyl Cellulose (CMC) in water rather than with PolyVinylidene diFluoride (PVdF) in *N*-Methyl-2-Pyrrolidone (NMP), X-ray Photoelectron Spectroscopy (XPS) and electrochemical tests have been carried out to carefully investigate the chemical composition of the SEI layer formed at the Sb electrode surface in the Li- and Na-system, with the different binders. Sb electrodes were cycled using a standard EC/PC/3DMC (1 M $LiPF_6$) electrolyte containing Vinylene Carbonate (VC) and FluoroEthylene Carbonate (FEC) for Li system and a standard Propylene Carbonate PC (1 M $NaClO_4$) electrolyte containing FEC for Na system. Surface analysis was performed by a combined XPS core peaks and quantification data analysis to establish the main components of the Solid Electrolyte Interphase film (SEI). The key observation is that the thickness of the SEI layer is strongly related to the nature of the polymer binder used in the formulation and that its chemical nature is different in Li and Na batteries. Much favorable SEI in the case of Sb-CMC/Na seems to participate to the excellent performance of this electrode.

1. Introduction

Rechargeable Li-ion batteries (LIBs) have been widely used for various portable applications due to their high energy densities [1]. Recently, sodium (Na)-ion batteries (NIBs) have attracted wide attention as an alternative to Li-ion batteries (LIBs) [2–7], in particular for large-scale energy storage applications as perspective. Alloy-based materials usually provided much higher gravimetric and volumetric specific capacities compared to carbonaceous materials for LIBs and as recently demonstrated for NIBs as well. Although high-capacity alloying anodes have undergone intensive development for LIBs, little research has still been done for alloy-based anode materials for NIBs. For LIBs, the difficulty to stabilize the capacity upon long cycling of alloy-based materials (Si, Sn, etc.) has been attributed to the lithiation-/delithiation-induced volume change. Since the sodium ion possesses a larger radius than the lithium ion, the effect of volume change upon sodiation/desodiation should be even more severe for the application of alloy-based materials in NIBs [8]. Thus, the development of stable alloy-based anode materials for NIBs is expected to be more

* Corresponding author. IPREM-ECP CNRS UMR 5254, Université de Pau, Hélioparc Pau Pyrénées, 2 av. Pierre Angot, 64053 Pau Cedex 9, France.
Tel.: +33 5 59407599; fax: +33 5 59407622.
E-mail address: herve.martinez@univ-pau.fr (H. Martinez).

http://dx.doi.org/10.1016/j.jpowsour.2014.09.037
0378-7753/

challenging than for LIBs [8,9]. Despite this pessimistic projection, few alloy-based materials [10–12], SnSb [13–15], Cu_2Sb [16,17], AlSb [18], $FeSb_2$ [19] and as well as metallic Sb or Sn oxides, Sb_2O_4 [20] have recently shown good performance for NIBs [12,15,21,22]. Among them antimony (Sb) appears to be the best candidate, since even under micrometric powder form it can sustain over hundred cycles against Na a capacity close to 600 mAh g^{-1} at a high rate with a good coulombic efficiency [23].

In LIBs, the cycling performance is strongly associated to the quality of the SEI layer, which has been shown to be depended on the structural change of the active material during cycling [24–27]. The latter is a very critical point in the case of conversion reactions, which are interface driven and go through the continuous restructuration of the electrode material. The same is true for the alloying reaction, for which the electrochemical grinding produces a new exposed surface that might negatively interact with the electrolyte [23].

In NIBS, the higher value of the Na^+/Na potential compared to Li^+/Li is expected to reduce electrolyte degradation at the surface of the electrode material. Up to now, there have been limited fundamental explorations on the formation of the SEI layer for Na^+ storage materials [4,21,28]. Since the formation of SEI layer plays a crucial role in the cycling ability of the electrode, it is very important to understand the mechanism which leads to its formation as well as the composition of this layer.

Moreover in LIBs and in NIBs, the electrode formulation and the choice of the associated binder are critical for the conductivity properties enhancement and further performances.

The most used polymers during the last few years are a combination of PolyVinylidene Fluoride (PVdF) and *N*-Methyl-Pyrrolidone (NMP) as solvent or a combination of CarboxyMethyl Cellulose (CMC) in water as solvent. It has been reported that the good electrochemical performance of metalloïds (Sb, P…) based negative electrode material in Li-ion batteries are correlated with the formulation with the carboxymethyl cellulose binder [29,30].

To understand the reason of the best performance of Sb electrode against Na than against Li and with CMC rather than with PVdF as binder we have decided to explore the SEI in these different cases. In this study, X-ray Photoelectron Spectroscopy (XPS) and electrochemical tests were carried out to carefully investigate the chemical composition of the SEI layer formed at the Sb electrode surface in the Li- and Na-system with two different binders, CMC and PVdF.

2. Experimental details

2.1. Preparation of the electrodes and electrochemical characterization

The electrochemical performances of Sb as negative electrode materials were examined in a standard coin cells assembled in an argon-filled glove box. The micrometric powder of antimony used in this study was provided by Alfa-Aesar (99.5% purity, ~325 mesh), and has been used without any additional treatment.

Electrode formulation was made using a mixture of carbon black and vapor ground carbon fibers (VGCF-S) as conductive additive, and carboxymethyl cellulose (CMC) (DS = 0.7, Mw = 250,000 Aldrich) for the formulation in water and polyvinylidene fluoride (PVDF) for the formulation in *N*-Methyl-2-pyrrolidone (NMP), as the binder. A slurry containing 70 wt.% active material, 12 wt.% binder and 18 wt.% conductive additive was homogeneously mixed by a planetary ball-milling for 1 h, tape casted on a 150 μm thick copper foil, dried at room temperature for 12 h and finally at 100 °C under vacuum for another 2 h. The final mass loading of active material on the electrode was 2 mg cm^{-2}.

The electrochemical tests vs Na or Li were performed against a counter-electrode of the corresponding pure metal, using either 1 M $NaClO_4$ in PC: 5% FEC or 1 M $LiPF_6$ in EC:PC:3DMC:1% VC (vinylene carbonate) and 5% FEC (FluoroEthylene Carbonate), as the electrolyte, respectively. Whatman glass-fiber was used as separator. All tests were carried out at room temperature (25 °C) using a multichannel VMP system under galvanostatic mode from 0.02 to 1.5 V vs Li^+/Li or vs Na^+/Na at C/2 rate (i.e. 0.5 Li or Na in one hour).

For XPS analysis, the electrodes were recovered from the coin cell, washed with pure DMC and dried under vacuum.

2.2. XPS

XPS measurements were carried out with a Thermo Scientific K-Alpha X-ray photoelectron spectrometer, using a focused monochromatized Al Kα radiation ($h\nu = 1486.6$ eV). The XPS spectrometer was directly connected through a glove box under argon atmosphere, in order to avoid moisture/air exposure of the samples. For the Ag $3d_{5/2}$ line the full width at half-maximum (FWHM) was 0.50 eV under the recording conditions. The X-ray spot size was 400 μm. Peaks were recorded with constant pass energy of 20 eV. The pressure in the analysis chamber was less than 2×10^{-7} Pa. Short acquisition time spectra were recorded at the beginning and at the end of each experiment to check that the samples did not suffer from degradation during the measurements. Peak assignments were made with respect to reference compounds analyzed in the same conditions. The binding energy scale was calibrated from the hydrocarbon contamination using the C 1s peak at 285.0 eV. Core peaks were analyzed using a nonlinear Shirley-type background [31]. The peak positions and areas were optimized by a weighted least-squares fitting method using 70% Gaussian, 30% Lorentzian line shapes. Quantification was performed on the basis of Scofield's relative sensitivity factors [32]. Sb electrodes were thoroughly rinsed with pure DMC and dried before XPS measurements; it is assumed that there was no trace of $LiPF_6$ or $NaClO_4$ salt and solvents left at the electrode surface during these measurements. For each electrode sample, several XPS analyses were performed at different positions to make the results statistically reliable.

3. Electrochemical properties of Sb electrode

Fig. 1 shows the galvanostatic curve of Sb electrode cycled versus lithium and sodium at C/2 rate (0.5 mol of Na or Li per

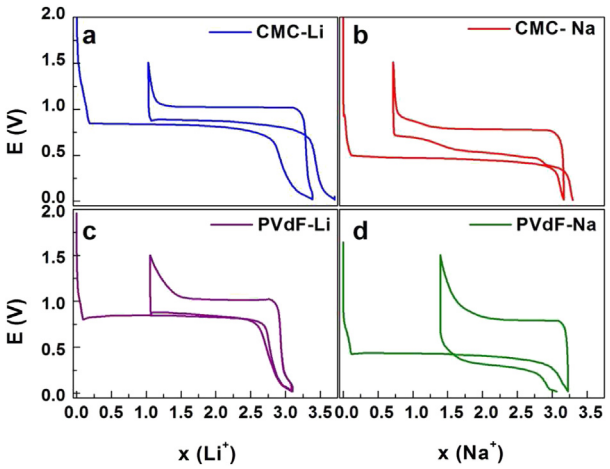

Fig. 1. Composition–voltage profile for Sb-CMC/Li (left, top), Sb-PVdF/Li (left, bottom), Sb-CMC/Na (right, top) and Sb-PVdF/Na (right, bottom) cells cycled at C/2 rate between 1.5 and 0.02 V.

mole of Sb per hour, respectively) using CMC or PVdF as binder. In both case, the first lithiation or sodiation occurs on a single plateau at 0.81 V vs Li^+/Li and 0.45 V vs Na^+/Na. In our previous work [23], we have shown that, in the case of lithium with CMC formulation (Fig. 1a), a slight tail is visible when the potential gets close to 0 V at the end of the first insertion, probably representing the decomposition of the electrolyte at the electrode surface according to the number of inserted Li ions compared to the theoretical value of 3 (corresponding to the formation of Li_3Sb). This phenomenon is less pronounced when using PVdF as binder (Fig. 1c), which can be explained by the fact that there is less SEI formation in agreement with the number of inserted Li ions which is close to 3. Differently from the case of Li, with CMC formulation, no tail close to 0 V vs Na^+/Na is observed at the end of the first discharge, suggesting that at this working potential the electrolyte is less sensitive to decomposition than in the case of Li (Fig. 1b).

As we can see from the voltage profile, a poor reversibility is observed when using PVdF as binder in both cases and an increase in polarization is clearly identified (Table 1), in the case of sodium.

Table 1 shows the polarization and the irreversible at the first cycle for the four systems studied. In the case of lithium, the polarization is quite similar for CMC and PVdF. The difference is much more pronounced when cycling versus sodium with a value of 0.51 V and 0.25 V for PVdF and CMC, respectively. The irreversible capacity at the first cycle is also comparable for CMC and PVdF formulation when cycling versus lithium, which is not the case with sodium: the irreversible capacity of the PVdF formulation (43%) is twice the value (22%) of the CMC formulation.

Globally, the number of inserted ions is very close to the theoretical value of 3, corresponding to the formation of Na_3Sb in the case of sodium (with the CMC formulation). In the case of Li, the number of lithium ions inserted slightly exceeds 3, indicating that additional Li consumption occurs, most probably by parasitic electrolyte decomposition reactions. Moreover, antimony electrode formulated with the CMC as binder presents better performance than the electrode formulated with the PVdF, for Li^+ and Na^+ as well.

Fig. 2 shows the charge capacity and the cumulative losses plotted versus the cycle number with the electrode formulated with the CMC as binder. As discussed in our previous work, antimony presents a better electrochemical performance cycled versus sodium than that observed versus lithium. A sustainable capacity of 560 mAh g^{-1} for 100 cycles is observed when cycled with Na^+ while in the case of Li^+, a gradual drop is observed. If we take a look at the cumulative losses, we noticed a remarkable difference between the two systems. In the case of Na, a linear increase is clearly identified during cycling which is not the case with Li, where a strong increase in the cumulative losses is observed during the first ten cycles, followed by a linear increase in the next cycles.

To better understand the effect of the SEI layer on the electrochemical performance of these electrodes, XPS analyses were performed in order to identify the composition and the thickness of this layer.

Table 1
Polarization (volts) and Irreversible capacity at the 1st cycle for the 4 cells studied.

Formulation	Polarization (V)[a]	Irreversible 1st cycle
CMC_Li	0.16	30%
CMC_Na	0.25	22%
PVdF_Li	0.18	34%
PVdF_Na	0.51	43%

[a] Difference between the potential at the half of the $(n + 1)$ charge and the potential at the half of the (n) discharge.

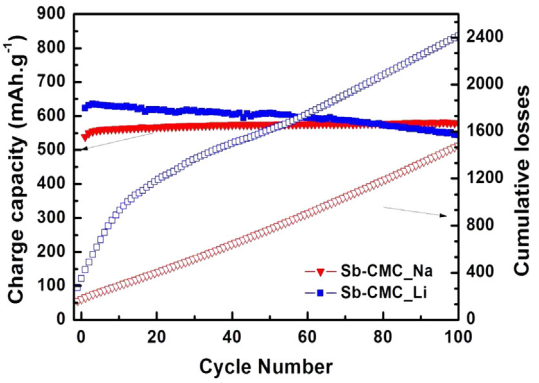

Fig. 2. Charge capacity and cumulative losses plotted versus the cycle number for Sb-CMC electrode vs Li (□) and vs Na (▼).

4. Surface analysis results

4.1. Sb-PVdF and Sb-CMC reference electrodes

Sb 3d and O 1s XPS core peaks of antimony powder and of fresh electrodes made of antimony, carbonaceous additives and of CMC or PVdF binder are presented in Fig. 3. Because of the overlapping of Sb 3d and O 1s core peaks, Sb 3d spectrum is fitted according to area and energy splitting (9 eV) constraints between $3d_{5/2}$ and $3d_{3/2}$ components. Two main components are clearly detected in the three spectra; they are identified by two peaks at 528.5 ($3d_{5/2}$) and 537.5 eV ($3d_{3/2}$) for metallic Sb and 531 ($3d_{5/2}$) and 540 eV ($3d_{3/2}$) for Sb_2O_3. The strong presence of antimony oxide is probably due to the oxidation of the Sb particle surface.

The component at 530.5 eV is attributed to the Sb_2O_3 oxide in the O 1s core peak.

Table 2 reports (in its first columns) the atomic percentages of antimony and oxygen attributed to Sb° and Sb_2O_3 and of carbon attributed to the carbonaceous additives measured by XPS. The

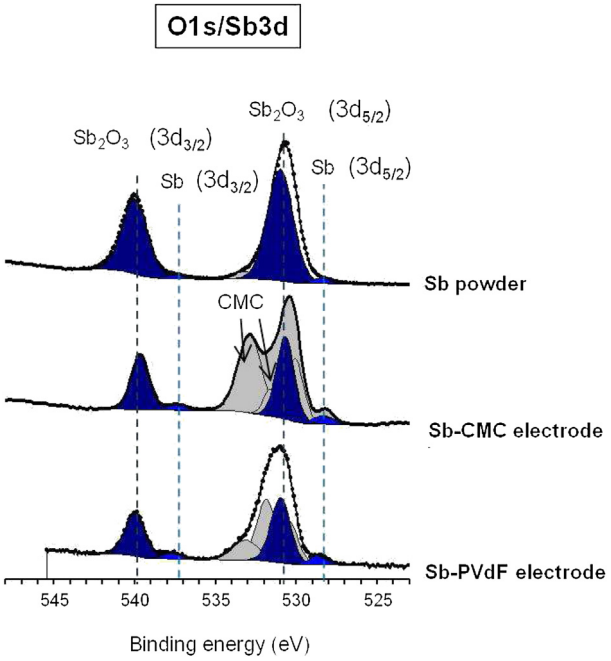

Fig. 3. The XPS O 1s and Sb 3d core peaks spectra of antimony powder and of the reference electrodes formulated with antimony and CMC or PVdF binder.

Table 2
XPS atomic percentages of antimony and oxygen attributed to the active material, of carbon from the carbonaceous additives and of a) fluorine and carbon attributed to the PVdF binder for the PVdF-based electrode, b) Na from the CMC binder for the CMC-based electrode, at different stages of discharge (1/2D1, 2/3D1 and D1) and charge (C1) during cycling versus lithium. B.E. stands for "binding energy" (eV).

a)

		Fresh Sb-PVdF		1/2D1 Sb-PVdF vs Li		2/3D1 Sb-PVdF vs Li		D1 Sb-PVdF vs Li		C1 Sb-PVdF vs Li	
		B.E. (eV)	At. %	B.E. (eV)	At. %	B.E. (eV)	At. %	B.E. (eV)	At. %	B.E. (eV)	At. %
Sb°	Sb3d	528.7–537.7	*<0.1*	–	–	–	–	–	–	–	–
Sb_2O_3	Sb 3d	531–540	0.5	–	–	–	–	–	–	–	–
	O 1s	530.5	1.6	–	–	–	–	–	–	–	–
			2.1	–	–	–	–	–	–	–	–
PVdF	C 1s	290.9	4.8	290.8	2.4	290.9	3	291.3	1.8	291.3	2
	F 1s	687.7	5.1	688.1	3.8	688.2	4.1	688.4	2.9	688.4	3.4
Carbonaceous additive	C 1s	284.5	*43.4*	–	–	–	–	–	–	–	–

b)

		Fresh Sb-CMC		1/2D1 Sb-CMC vs Li		2/3D1 Sb-CMC vs Li		D1 Sb-CMC vs Li		C1 Sb-CMC vs Li	
		B.E. (eV)	At. %	B.E. (eV)	At. %	B.E. (eV)	At. %	B.E. (eV)	At. %	B.E. (eV)	At. %
Sb°	Sb3d	528.3–537.3	*0.2*	–	–	–	–	–	–	528.3–537.3	*0.05*
Sb_2O_3	Sb 3d	530.7–539.7	1.7	–	–	–	–	–	–	–	–
	O 1s	530.1	6	–	–	–	–	–	–	–	–
			7.7	–	–	–	–	–	–	–	–
Na (from CMC-Na)	Na 1s	1071.8	*6.2*	1072.1	*0.1*	–	–	–	–	1072.2	*0.2*
Carbonaceous additive	C 1s	284.3	*28.3*	–	–	–	–	–	–	284.0	*5.2*

atomic percentages of carbon and fluorine attributed to the PVdF binder (Table 2a) and of sodium from the CMC binder (Table 2b) are also reported.

The characteristic peaks of the oxide and of metallic antimony are observed in the same relative proportions in the CMC-based and in the PVdF-based antimony electrodes. The main difference between the two spectra lies in the O 1s core peak, where the two characteristic components of the CMC binder are observed: at 533 eV (C–O–C) and 531.6 eV (O–C=O) [33].

4.2. Nature and thickness of the passivation layer of the Sb electrode vs Li

The chemical nature of the passivation layer can be studied by X-ray Photoelectron Spectroscopy (XPS) which offers a global view of the surface layer with a 5 nm thickness. The analyses were directly performed on fresh electrodes cycled at different stages of discharge and charge. Several XPS core peaks and valence bands spectra are presented in the following results.

Tables 2 and 3 also summarize the XPS results: Table 2a reports the atomic percentages of all the component of the reference electrode (active material, PVdF binder and carbonaceous additives), and the atomic percentages of these components detected at different stages of discharge and charge when cycling versus lithium. The evolution of these percentages is a reliable indicator of the electrode covering by the passivation layer. Table 2b reports the equivalent data concerning the Sb-CMC based electrode cycled versus lithium, and Table 3 for cycling versus sodium.

The atomic percentages of all the species forming the SEI detected by XPS, for cycling versus Li and versus Na, are reported in quantification tables in supplementary information.

Table 3
XPS atomic percentages of antimony and oxygen attributed to the active material, of carbon from the carbonaceous additives and of a) fluorine and carbon attributed to the PVdF binder for the PVdF-based electrode, b) Na for the CMC-based electrode, at different stages of discharge (1/2D1, 2/3D1 and D1) and charge (C1) during cycling versus sodium. B.E. stands for "binding energy" (eV).

a)

		Fresh Sb-PVdF		1/2D1 Sb-PVdF vs Na		2/3D1 Sb-PVdF vs Na		D1 Sb-PVdF vs Na		C1 Sb-PVdF vs Na	
		B.E. (eV)	At. %	B.E. (eV)	At. %	B.E. (eV)	At. %	B.E. (eV)	At. %	B.E. (eV)	At. %
Sb	Sb3d	528.7–537.7	*<0.1*	–	–	–	–	–	–	–	–
Sb_2O_3	Sb 3d	531–540	0.5	–	–	–	–	–	–	–	–
	O 1s	530.5	1.6	–	–	–	–	–	–	–	–
			2.1	–	–	–	–	–	–	–	–
PVdF	C 1s	290.9	4.8	290.7	0.8	290.5	3.6	290.6	3.8	290.8	1.6
	F 1s	687.7	5.1	688.0	3.4	687.9	3.5	687.9	4	687.8	3.9
Carbonaceous additive	C 1s	284.8	*43.4*	284.0	*10.2*	–	–	–	–	–	–

b)

		Fresh Sb-CMC		1/2D1 Sb-CMC vs Na		2/3D1 Sb-CMC vs Na		D1 Sb-CMC vs Na		C1 Sb-CMC vs Na	
		B.E. (eV)	At. %	B.E. (eV)	At. %	B.E. (eV)	At. %	B.E. (eV)	At. %	B.E. (eV)	At. %
Sb°	Sb 3d	528.3–537.3	*0.2*	–		–		–		528.1–537.1	*0.7*
Sb_2O_3	Sb 3d	530.7–539.7	1.7	–	–	–	–	–	–	530.4–539.4	0.5
	O 1s	530.1	6	–	–	–	–	–	–	530.0	1.9
			7.7	–	–	–	–	–	–		*2.4*
Na (total)	Na 1s	**1071.8**	*6.2*		*35.2*		25.3		46.3		*19.2*
Carbonaceous additive	C 1s	284.3	*28.3*	283.8	*2.4*	283.6	*1*	283.3	*0.3*	283.8	*18.8*

4.2.1. Sb-PVdF electrode cycled versus Li

Sb 3d/O 1s and C 1s core peaks are presented in Fig. 4. As noted previously, two components are clearly detected in the Sb-PVdF reference electrode: metallic Sb (528.5–537.5 eV) and Sb_2O_3 (531–540 eV). At the half of the first discharge, the peaks corresponding to metallic and oxidized Sb are no more detected neither at the end of the discharge, nor at the end of the first charge. This result indicates that the SEI layer formed on the active material is thicker than 5 nm, which is the depth limit of the XPS analysis. The C 1s spectrum of the reference electrode (Fig. 4b) displays an intense peak at 284.5 eV corresponding to the carbonaceous additives. This component is no longer detected on the cycled electrode, indicating that the carbonaceous additives are also covered by a passivation layer thicker than 5 nm. A small peak displayed at 291 eV is observed, which is characteristic of the $\underline{C}F_2$–CH_2 environment in the PVdF binder. The peak assigned to the carbon atom in $\underline{C}H_2$–CF_2 is observed at 286.4 eV [34]. The component at 291 eV is detected on the C 1 core peaks of all the cycled electrodes (discharged and charged): the decomposition products of the electrolyte do not seem to form a thick SEI on the PVdF binder, but only on the active material and the conductive additives.

The XPS F 1s core peaks (Fig. 5) also show that the PVdF binder (at 687.7 eV) is detected all over the discharge and also at the end of the charge. This observation confirms that the passivation layer does not homogeneously cover the active material and the binder. The XPS C 1s core peaks spectra of the electrode formulated with PVdF binder presented in Fig. 4 also provide valuable information regarding the SEI nature. The component with a binding energy of 285.0 eV in C 1s spectra is assigned to CH_x environment, which is attributed to hydrocarbon contamination (always detected at the extreme surface) and to carbon atoms of organic species bound to carbon or hydrogen atoms only. The component observed at 286.5 eV can be assigned to carbon atoms bound to one oxygen atom (C–O), while the component at 289.0 eV corresponds to carbon atoms bound to two oxygen atoms (O=C–O) [35]. The component observed at 290.2 eV is characteristic of carbon bound to three oxygen atoms, which is typical of carbonate-like species ($-CO_3$) that could be Li_2CO_3 or lithium alkyl carbonates $ROCO_2Li$ [36,37]. An increase of the relative intensity of the component associated with carbon atoms in C–O bonds is observed all over the discharge. These ether groups may be attributed to PEO, which is classically formed in the SEI when cycling with an EC-based electrolyte [38].

The F 1s core peaks of cycled electrodes are characterized by three main components at 685.2, 686.5 and 688 eV, which can be assigned to LiF, $LiPF_6$ and PVdF, respectively. The P 2p core peaks also shown on Fig. 5 have been fitted by considering two resolved doublets (with a spin-orbit splitting of 0.9 eV between $2p_{3/2}$ and $2p_{1/2}$). They are characterized by a broad peak consisting of three main components at 134.2, 136 and 138 eV which corresponds to phosphates, fluorophosphates and $LiPF_6$, respectively [39].

From the beginning of the reaction of Sb with lithium and until the end of the first discharge, the composition of the SEI remains stable: it is mainly formed of carbonates (from the decomposition of the solvent of the electrolyte), $LiPF_6$, LiF, and fluorophosphates (from the decomposition of the electrolyte salt). During the charge, the amount of LiF decreases from 8 to 3% which can be explained by a partial dissolution of the SEI layer, leading to a better detection of C–O components (see Table 1 in supplementary data).

4.2.2. Is the SEI layer of the Sb electrode vs Li formulated with the CMC binder in water is similar to that with the PVdF binder in NMP?

To answer this question, we performed the same XPS analysis done on the previous system on the Sb electrode formulated with CMC.

Fig. 6 shows the XPS C 1s, O 1s/Sb 3d core peaks of the Sb reference electrode, of the electrode during discharge and at the end of the charge.

The XPS O 1s and Sb 3d spectra shown in Fig. 6a reveal that, like in the case of PVdF, the Sb active material is covered from the middle of the first discharge until the end of the discharge, indicating the formation of a thick SEI layer (more than 5 nm). However, the active material is detected again at the end of charge, which is the consequence of a partial dissolution of the SEI. However, it should be noted that only Sb° is observed, whereas it was mostly Sb_2O_3 on the starting electrode.

Table 2b shows the atomic percentage of Na detected at the surface of the fresh electrode Sb/CMC and of the cycled electrode by XPS. The presence of Na results from the use of the CMC binder and is a good probe to estimate its covering along cycling: the atomic percentage of Na decreases from 6.2% (on the fresh electrode) to 0.1% on the 1/2D1 sample, indicating that the binder is almost

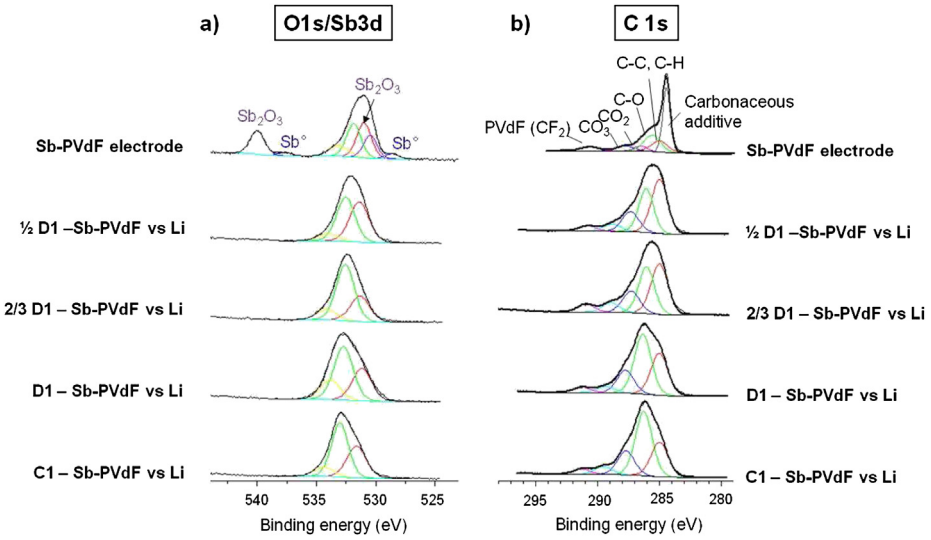

Fig. 4. a) The XPS O 1s and Sb 3d core peaks and b) C 1s core peaks spectra of the Sb-PVdF electrode at different stages of the first cycle vs Li (1/2D1, 2/3D1, D1 and C1). The spectra of the reference electrode are also presented.

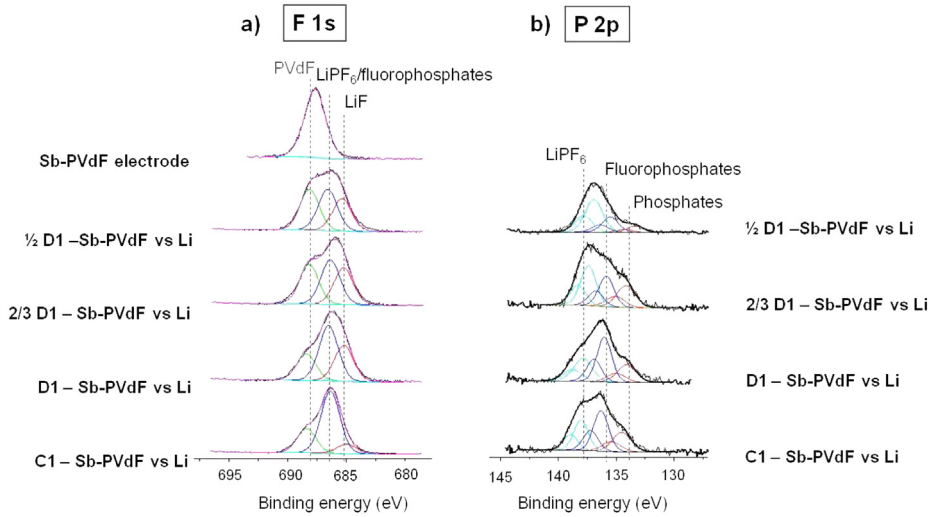

Fig. 5. a) The XPS F 1s core peaks and b) P 2p core peaks spectra of the Sb-PVdF electrode at different stages of the first cycle vs Li (1/2D1, 2/3D1, D1 and C1). The spectrum of the reference electrode is also presented.

completely covered by the passivation layer at this stage of discharge. It is no longer observed on 2/3D1 and D1 samples. It is detected again (in small amount) at the end of the charge, similarly to the active material. Fig. 6b displays the valence band of each electrode during cycling, mostly corresponding to the ionization of Na 2p and Sb 4d orbitals. The Na 2p component, corresponding to the CMC binder, decreases during the discharge, indicating a progressive overlap of the binder by the SEI layer. However, the Sb active material is no longer detected from the half of the first discharge. At the end of the first charge, the Sb active material and the Na 2p peak of the binder are detected again which confirms the partial dissolution of the SEI. It should be noticed that in this range of binding energy, we probe the material with a slightly greater depth than during Na 1s, O 1s and Sb 3d core peaks analysis, because the kinetic energy of the electrons of the valence band is greater.

At the middle of the discharge, at the 2/3 and at the end of the discharge, the O 1s/Sb 3d spectra are mainly consisting of two components, namely LiOH and Li_2O (between 50 and 60% – see Table 2 in supplementary data). These latter are present before the XPS analysis, probably because of the electrode formulation in water. Several tests are done at the beginning and the end of the analysis, in order to identify if the Li_2O species is one of the SEI components or if it is a degradation product of LiOH under the X-ray beam. No change was observed before and after analysis in each electrode which confirms that the Li_2O species is one of the SEI major components.

The XPS C 1s core peak spectra show mainly C–C and C–H environments, with a small amount of C–O for 1/2D1, 2/3D1 and end of the D1 samples, and with no trace of $-CO_3$ and $-CO_2$ environments. These latter appear at the end of the charge, probably because of the dissolution of Li_2O/LiOH species during the charge: their amount drops down to 15% at the surface of the electrode at the end of the charge. Few or no fluorinated species are present in the case of Sb electrode formulated with CMC. Only LiF (16%) is detected at the end of the charge. The composition of the SEI layer is clearly different than that of the previous system.

To summarize, concerning the nature of the SEI layer formed, in the case of Sb-PVdF system, a classical chemical composition is observed considering the electrolyte used (solvent EC, PC and DMC

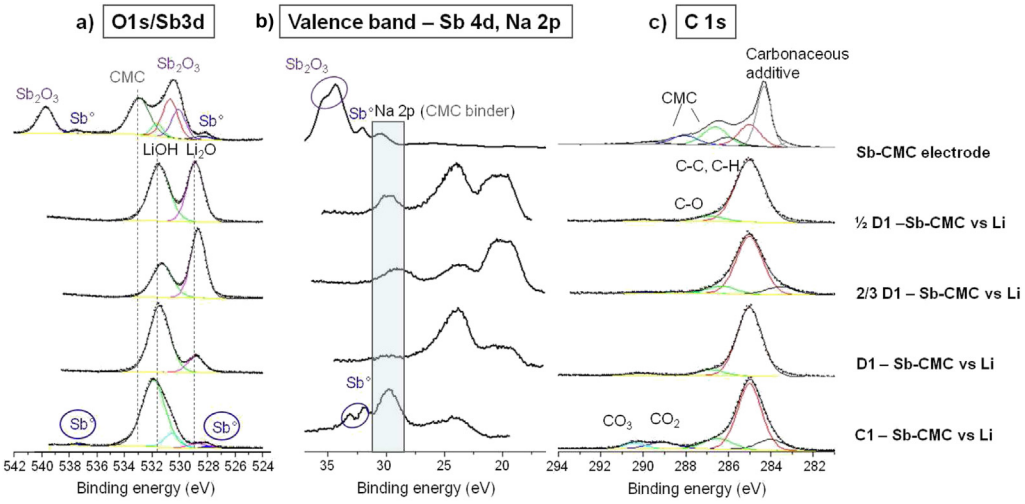

Fig. 6. a) The XPS O 1s and Sb 3d core peaks spectra. b) The valence band and c) C 1s core peaks spectra of the Sb-CMC electrode at different stages of the first cycle vs Li (1/2D1, 2/3D1, D1 and C1). The spectra of the Sb reference electrode are also presented.

and $LiPF_6$ lithium salt), since the degradation products detected are those of solvents (−CO, $-CO_2$, $-CO_3$ environments), and those of the $LiPF_6$ salt (LiF, fluorophosphates and phosphates). Although the active material is not detected at the end of the charge, the decrease of the content of LiF and of species with a C−O bond allows considering a slight dissolution of the SEI. In the case of electrodes made with the binder CMC, most of the species mentioned above are not detected by XPS during the discharge. Only C−C, C−H and C−O environments in small proportion and few fluorinated and/or no phosphorus species were observed. The main compounds detected by XPS in the discharge are LiOH and Li_2O. Their presence is probably due to the use of water in the formulation of the electrodes with the CMC binder. These species are detected in much lower amounts at the end of the charge, in favor of carbon species and LiF.

Concerning the thickness and the morphology of the SEI layer, in the case of PVdF, the active material (Sb) is no longer detected from the half of the first discharge and is not re-detected at the end of the charge: on all the analyzed samples, the SEI covers the active material with a thickness greater than the depth of analysis of XPS (about 5 nm). However the increase of the amount of LiF after charging allows considering a slight dissolution of at least a portion of species of the passivation layer. The observation of C 1s and F 1s core peaks also indicates that the PVdF binder is detected throughout the discharge and at the end of the charge, and thus does not seem covered by the SEI, which appears to be preferentially formed on the active material.

In the case of CMC binder, as in the case of PVdF, antimony is covered from the half of the first discharge. The analysis of Na 1s and Na 2p core peaks indicates a progressive covering of the binder by the passivation layer during the discharge. Unlike the previous system, the dissolution of the SEI during the charge (probably of $LiOH/Li_2O$ species) allows the detection of the active material and of the binder after charging. The thickness of the SEI is then less than 5 nm. It appears to cover the surface of the electrode more homogeneously than the passivation layer formed at the Sb-PVdF electrode's surface.

4.3. Nature and thickness of the passivation layer of the Sb electrode cycled vs Na

The analyses were performed on the same fresh electrodes than vs Li, cycled at the same stages of discharge and charge which allow the comparison of electrode/electrolyte interfaces. The electrolyte used in the case of cycling vs Na was $NaClO_4$ (sodium salt) in PC (solvent) with 5% FEC (as additive).

4.3.1. Sb-PVdF vs Na

On Fig. 7a (O 1s/Sb 3d), upon the half of the first discharge (1/2D1), the antimony is not detected. It should be noted that during cycling vs sodium, two Na Auger transition peaks appear at 536 and 523 eV.

However, in the C 1s core peak of the same sample (Fig. 7b), the component located at 284.3 eV, characteristic of the carbonaceous additives, is still detected. The peaks corresponding to the PVdF binder, located at 291 (C 1s) and 688 eV (F 1s), are observed all over the first cycle. This observation suggests that the passivation layer formed is discontinuous and covers preferentially the active material and the carbon additive at the expense of the PVdF binder.

At the half of the first discharge, a new component located at 684.3 eV appears on the F 1s core peak spectra (Fig. 8a), corresponding to the deposition of NaF at the electrode's surface. This observation is in agreement with Baggetto study [40] on Sb thin films cycled in the presence of FEC. According to their study, these species confer desirable properties in terms of lifetime to Na-ion batteries cycled with this additive. This species is formed at the beginning of the discharge and does not seem to re-dissolve during the charge. Fig. 8b shows the XPS Cl 2p core peak spectra of the Sb-PVdF electrode, which indicates a partial reduction of the electrolyte salt to NaCl and $NaClO_3$ at the electrode surface. A part of this reduction may be due to X-ray beam as the relative intensity of the NaCl component increases during the acquisition of the XPS spectra. This reduction of the salt is, however, also due to electrochemical processes because this component is present from the start of the XPS acquisition.

The amount of $NaClO_x$-type compounds remains stable during the discharge and the charge (6−7%). At the end of the charge, the amount of carbonates and of compounds with a $-CO_2$ group slightly decreases in favor of organic species with C−C, C−H bonds (see Table 3 in supplementary data). Neither the active material nor the carbonaceous additives are detected at the end of the first charge, meaning that they are covered with a passivation layer thicker than 5 nm (but possibly discontinuous at the PVdF binder).

4.3.2. Sb-CMC vs Na

Figs. 9 and 10 show the XPS Cl 2p, F 1s, Na 1s, O 1s/Sb 3d and the valence band of Sb electrode formulated with the CMC as binder and

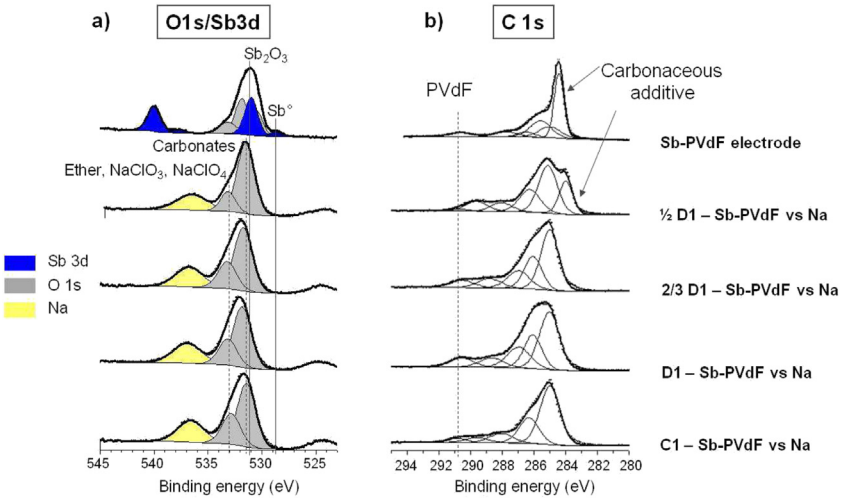

Fig. 7. a) The XPS O 1s and Sb 3d core peaks and b) C 1s core peaks spectra of the Sb-PVdF electrode at different stages of the first cycle vs Na (1/2D1, 2/3D1, D1 and C1). The spectra of the reference electrode are also presented.

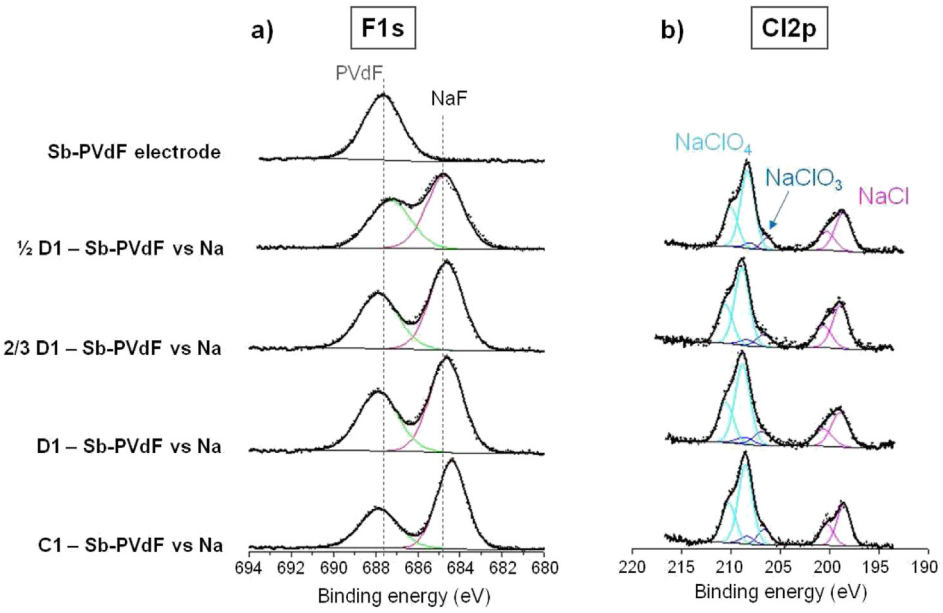

Fig. 8. a) The XPS F 1s core peaks and b) Cl 2p core peaks spectra of the Sb-PVdF electrode at different stages of the first cycle vs Na (1/2D1, 2/3D1, D1 and C1). The spectrum of the reference electrode is also presented.

cycled versus sodium. The Sb 3d core peak spectra (Fig. 9a) show, as in the case of the Sb-PVdF system, that the active material is covered by a passivation layer from the half of the first discharge. However, unlike the previous system, the carbon additive (C 1s core peak) and the CMC (O 1s core peak) are no longer detected. The main difference between this system and the previous one is the detection, at the end of the first charge, of antimony characteristic peaks, reflecting a partial re-dissolution of the SEI during charging. This dissolution is not complete because, as observed in Table 3b, more antimony is measured at the surface of the starting electrode (1.9%) compared with the end of the charge (1.2%). The characteristic peak of carbon additives is also detected again in large amounts on the C 1s core peak spectra at the end of the charge.

It should be noted that, due to the overlap of all the components in O 1s (Fig. 9a) and Na 1s core peaks (Fig. 10c), it is difficult to obtain an accurate quantification of all the species in the SEI (Table 4 in supplementary data). However, being given the global amounts of Na and the shoulder at low binding energy on the Na 1s core peaks (for 1/2D1, 2/3D1 and D1 samples), we can suppose that a significant amount of Na_2O and possibly NaOH is formed at the electrode surface during discharge. These species would dissolve during the charge, leading to the detection of NaF (15%) as observed on Fig. 10b. This phenomenon is similar to the cycling vs Li, but with less NaOH/Na_2O formed compared to LiOH/Li_2O.

The observation of the Sb 3d core peak also provides information about the oxidation state of antimony at the end of charge:

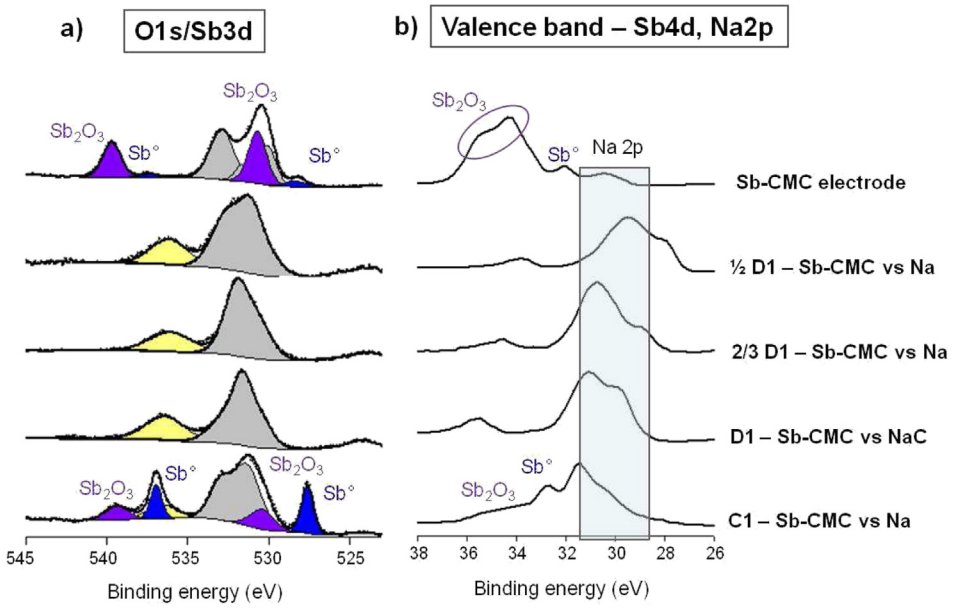

Fig. 9. a) The XPS O 1s and Sb 3d core peaks and b) valence band of the Sb-CMC electrode at different stages of the first cycle vs Na (1/2D1, 2/3D1, D1 and C1). The spectra of the reference electrode are also presented.

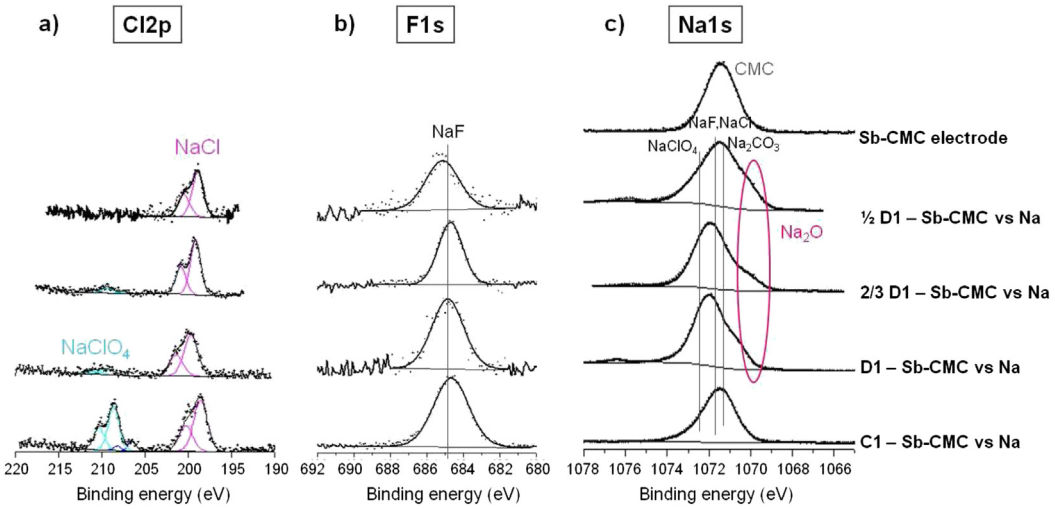

Fig. 10. a) The XPS Cl 2p core peaks, b) F 1s core peaks and c) Na 1s core peaks spectra of the Sb-CMC electrode at different stages of the first cycle vs. Na (1/2D1, 2/3D1, D1 and C1). The spectrum of the reference electrode is also presented.

compared with Sb 3d core peak of the reference electrode, the two same doublets are observed, attributed to Sb° and to Sb_2O_3. However, the ratio between the two species is different as Sb° is detected in a larger amount than Sb_2O_3 (Table 3b). This observation suggests a complete conversion of Na_3Sb (formed at the end of the discharge) to Sb° during the charge.

The total covering of the active material by the passivation layer during discharge does not allow the observation by XPS of the signature neither of the "expected" amorphous phase Na_xSb during discharge nor of the Na_3Sb phase at the end of the discharge.

In agreement with the literature, in the case of Na–Sb/CMC and Na–Sb/PVdF systems, the SEI formed on the surface of the antimony electrodes is made of sodium salt ($NaClO_4$) and its degradation products $NaClO_3$ and NaCl [41]. We also noted the formation of NaF, due to the presence of the additive FEC. This species does not re-dissolve during the charge. The degradation of the electrolyte solvents also results in the formation of sodium carbonate Na_2CO_3 or $ROCO_2Na$. In the case of system Na–Sb/CMC, the presence of Na_2O is noted at the surface of the sample at the half of the first discharge. It is consistent with the use of water during the formulation of an electrode with CMC binder.

The difference between the Sb-CMC and the Sb-PVdF systems studied versus sodium lies rather in the thickness and homogeneity of the SEI formed at the surface of the electrodes analyzed by XPS: in both cases, the passivation layer is covering the active material (Sb) at the half of the first discharge. While the binder CMC is also covered at the beginning of the first discharge, the PVdF binder is detected throughout cycling. These observations suggest the formation of a discontinuous (inhomogeneous) passivation layer in the case of the electrode formulated with the PVdF as binder.

At the end of first charge, the antimony is detected by XPS at the surface of the Sb-CMC electrode, resulting from a partial re-dissolving of the passivation layer during charge (dissolution of Na_2O/NaOH). Instead, antimony is not detected at the surface of the Sb-PVdF electrode at the end of the first charge; in this case the passivation layer covering the active material still has a thickness greater than 5 nm.

4.4. Comparison of antimony electrodes cycled versus Li or Na

4.4.1. Comparison Sb-PVdF vs Li/Sb-PVdF vs Na

The carbon environments detected at the surface of the various samples analyzed are similar and characteristic of the degradation of the electrolyte's carbonate solvents used (PC in the case of sodium, PC: EC: DMC mixture in the case of lithium). The SEI is also composed of the degradation products of the electrolyte salt in both cases: – $NaClO_4$ for sodium system, leading to the detection of the salt itself as well as $NaClO_3$ and NaCl; – $LiPF_6$ for lithium system, leading to the detection of the salt, phosphates and fluorophosphates as well as the detection of LiF. In the case of cycling vs sodium, the FEC additive allows the formation of NaF which plays a role in the stabilization of the passivation layer. The active material is covered with a SEI layer with a thickness greater than 5 nm throughout cycling in both cases.

These observations are in agreement with the low performances in cycling and with the higher polarization which are observed for Sb-PVdF in Li as well as in sodium batteries.

4.4.2. Comparison Sb-CMC vs Li/Sb-CMC vs Na

While the passivation layers formed at the Sb-PVdF electrodes surface are comparable between Na and Li systems, significant differences exist (in terms of chemical nature) for the SEI formed at the surface of electrodes formulated with the Sb-CMC cycles versus Na, compared to Sb-CMC vs Li.

- The degradation products of the electrolyte salt ($NaClO_4$) were detected by XPS at the surface of the electrodes cycled versus Na, but few or no phosphorus/fluorinated species from the degradation of the $LiPF_6$ salt has been detected at the surface of the electrode cycled in Li system. These results are in agreement with Komaba studies [4], i.e. a more significant proportion of inorganic compounds exists at the surface of the electrodes cycled with Na^+, whereas the SEI of the electrodes cycled with Li^+ are mainly formed from hydrocarbons compounds.

- Little amount of NaOH/Na_2O has also been detected at the surface of the electrodes cycled in Na-ion system (despite the presence of H_2O in their formulation). In this case the passivation layer is also formed of carbonated species. On the contrary, high proportions of LiOH and/or Li_2O were measured at the surface of the electrodes in Li-ion system (during discharge).

The atomic percentage of active material measured by XPS at the end of the charge also provides information on the difference in thickness between the passivation layers at the end of discharge:

1.2 at.% of Sb is detected by XPS for the Na-ion system and only 0.05% for the Li-ion system. SEI is then thicker when the electrode is cycled versus Li; this difference in the thickness of the SEI between the two system was referred in the literature with an explanation that the potential Na^+/Na is higher than that of Li^+/Li, which would imply less degradation of the electrolyte at the surface of the electrodes. It may be also linked to the dissolution of the SEI species which is more pronounced in the case of electrodes cycled versus sodium during the charge [41].

It has to be noted that, in both case (vs Li or Na), the use of CMC as binder leads to the formation of a passivation layer that homogeneously covers the active material and the binder, on the contrary of the PVdF binder. During cycling vs Li and vs Na, less polarization and less irreversible are measured when using the CMC binder (compared to PVdF): the formation of a homogeneously thick SEI, obtained with the CMC binder, may contribute to obtain better electrochemical performances. In the case of cycling versus lithium, this result is in good agreement with the literature which reports the reactivity of the CMC binder toward the electrolyte [33] and which suggests that CMC chains can bind to Si via covalent or hydrogen bonding depending of the pH [42,43].

Less irreversible at the first cycle is obtained with CMC formulation, especially in the case of Na-system, where the irreversible is about 22%. This observation can be correlated to the XPS analysis: in the case of Sb-CMC/Li, the Sb 3d core peak corresponding to the antimony oxide (Sb_2O_3) is only visible for the reference electrode. It does not reappear at the end of charge, which is not the case for Sb-CMC/Na. The consumption of the antimony oxide in the case of the Sb-CMC/Li can be the reason of this higher irreversible.

Less polarization is also detected for Sb-CMC/Na. This result could be explained by the formation of a thinner SEI when the formulation with CMC is used. The tail observed at the end of the charge in the CMC-Li system confirms that the decomposition of the electrolyte also plays a key role in the formation of the SEI and is enhanced in the working potential of Li batteries. It should be noticed that the layer of antimony oxide observed by XPS, and which is not completely consumed during cycling, could limit the degradation of the electrolyte and the formation of the passivation layer.

In the other hand, the electrodes formulated with PVdF as binder show an important irreversible at the first cycle, i.e. 43% in the Sb-PVdF/Na system. A higher polarization is also observed with this latter. This phenomenon can be explained by the formation of a resistant and thicker layer at the surface of the electrode. From XPS analysis, this layer is thicker than 5 nm. The degradation of the electrolyte is more pronounced when using the PVdF binder, especially in the Na-system. The rapid increase in the cumulative losses during cycling in the Sb-CMC/Li system could be explained by the fact that more SEI is formed during the first ten cycles and which is more stable in the following cycles. However, in the case of Sb-CMC/Na, a linear increase was observed from the first cycles and remains linear until the end of the life of the battery (Fig. 2).

5. Conclusion

In this work, a systematic study of Sb electrodes cycled versus Li or versus Na has been carried out. Two electrode formulations have been compared in order to investigate the role of the binder (CMC or PVdF) on the battery performances. XPS studies highlighted the key role of the SEI in the good performances of Sb-CMC vs Na compared to the other systems: thanks to the formation of a thinner passivation layer, a smaller quantity of Na is irreversibly trapped leading to a better cyclability. We also demonstrated that the choice of the binder affects the thickness of the SEI, which is homogeneously formed on the active material, carbonaceous additives and on the CMC binder but not on the PVdF binder. Differences in the chemical composition of the passivation layer have been evidenced.

This work brings out the key-role of the SEI in the excellent performance of Sb or antimonides materials as negative electrodes in Na. These results show that a great effort has to be done in the direction of electrolyte and electrode formulation so that Na-ion batteries become a reality.

Acknowledgments

The RS2E (Réseau sur le Stockage Electrochimique de l'Energie) network is acknowledged for the financial support of A.D.

Appendix A. Supplementary data

Supplementary data related to this article can be found at http://dx.doi.org/10.1016/j.jpowsour.2014.09.037.

References

[1] P.G. Bruce, B. Scrosati, J.-M. Tarascon, Angew. Chem. Int. Ed. 47 (2008) 2930–2946.
[2] N.-S. Choi, Z. Chen, S.A. Freunberger, X. Ji, Y.-K. Sun, K. Amine, G. Yushin, L.F. Nazar, J. Cho, P.G. Bruce, Angew. Chem. Int. Ed. 51 (2012) 9994–10024.
[3] S.-W. Kim, D.-H. Seo, X. Ma, G. Ceder, K. Kang, Adv. Energy Mater. 2 (2012) 710–721.
[4] S. Komaba, W. Murata, T. Ishikawa, N. Yabuuchi, T. Ozeki, T. Nakayama, A. Ogata, K. Gotoh, K. Fujiwara, Adv. Funct. Mater. 21 (2011) 3859–3867.
[5] J. Liu, J.-G. Zhang, Z. Yang, J.P. Lemmon, C. Imhoff, G.L. Graff, L. Li, J. Hu, C. Wang, J. Xiao, G. Xia, V.V. Viswanathan, S. Baskaran, V. Sprenkle, X. Li, Y. Shao, B. Schwenzer, Adv. Funct. Mater. 23 (2013) 929–946.
[6] Y.-U. Park, D.-H. Seo, H.-S. Kwon, B. Kim, J. Kim, H. Kim, I. Kim, H.-I. Yoo, K. Kang, J. Am. Chem. Soc. 135 (2013) 13870–13878.
[7] M.D. Slater, D. Kim, E. Lee, C.S. Johnson, Adv. Funct. Mater. 23 (2013) 947–958.
[8] V.L. Chevrier, G. Ceder, J. Electrochem. Soc. 158 (2011) A1011–A1014.
[9] B.L. Ellis, L.F. Nazar, Curr. Opin. Solid State Mater. Sci. 16 (2012) 168–177.
[10] M.K. Datta, R. Epur, P. Saha, K. Kadakia, S.K. Park, P.N. Kumta, J. Power Sources 225 (2013) 316–322.
[11] L.D. Ellis, T.D. Hatchard, M.N. Obrovac, J. Electrochem. Soc. 159 (2012) A1801–A1805.
[12] Y. Xu, Y. Zhu, Y. Liu, C. Wang, Adv. Energy Mater. 3 (2013) 128–133.
[13] A. Darwiche, M.T. Sougrati, B. Fraisse, L. Stievano, L. Monconduit, Electrochem. Commun. 32 (2013) 18–21.
[14] L. Ji, M. Gu, Y. Shao, X. Li, M.H. Engelhard, B.W. Arey, W. Wang, Z. Nie, J. Xiao, C. Wang, J.-G. Zhang, J. Liu, Adv. Mater. 26 (2014) 2901–2908.
[15] L. Xiao, Y. Cao, J. Xiao, W. Wang, L. Kovarik, Z. Nie, J. Liu, Chem. Commun. 48 (2012) 3321–3323.
[16] L. Baggetto, E. Allcorn, A. Manthiram, G.M. Veith, Electrochem. Commun. 27 (2013) 168–171.
[17] L.c. Baggetto, K.J. Carroll, H.-Y. Hah, C.E. Johnson, D.R. Mullins, R.R. Unocic, J.A. Johnson, Y.S. Meng, G.M. Veith, J. Phys. Chem. C 118 (2014) 7856–7864.
[18] L. Baggetto, M. Marszewski, J. Gòrka, M. Jaroniec, G.M. Veith, J. Power Sources 243 (2013) 699–705.
[19] L. Baggetto, H.-Y. Hah, C.E. Johnson, C.A. Bridges, J.A. Johnson, G.M. Veith, Phys. Chem. Chem. Phys. 16 (2014) 9538–9545.
[20] Q. Sun, Q.-Q. Ren, H. Li, Z.-W. Fu, Electrochem. Commun. 13 (2011) 1462–1464.
[21] J. Qian, Y. Chen, L. Wu, Y. Cao, X. Ai, H. Yang, Chem. Commun. 48 (2012) 7070–7072.
[22] H. Zhu, Z. Jia, Y. Chen, N. Weadock, J. Wan, O. Vaaland, X. Han, T. Li, L. Hu, Nano Lett. 13 (2013) 3093–3100.
[23] A. Darwiche, C. Marino, M.T. Sougrati, B. Fraisse, L. Stievano, L. Monconduit, J. Am. Chem. Soc. 134 (2012) 20805–20811.
[24] Z. Jian, W. Han, X. Lu, H. Yang, Y.-S. Hu, J. Zhou, Z. Zhou, J. Li, W. Chen, D. Chen, L. Chen, Adv. Energy Mater. 3 (2013) 156–160.
[25] S.W. Lee, B.M. Gallant, H.R. Byon, P.T. Hammond, Y. Shao-Horn, Energy Environ. Sci. 4 (2011) 1972–1985.
[26] C. Marino, A. Darwiche, N. Dupré, H.A. Wilhelm, B. Lestriez, H. Martinez, R. Dedryère, W. Zhang, F. Ghamouss, D. Lemordant, L. Monconduit, J. Phys. Chem. C 117 (2013) 19302–19313.
[27] H. Pan, X. Lu, X. Yu, Y.-S. Hu, H. Li, X.-Q. Yang, L. Chen, Adv. Energy Mater. 3 (2013) 1186–1194.
[28] S. Komaba, T. Ishikawa, N. Yabuuchi, W. Murata, A. Ito, Y. Ohsawa, ACS Appl. Mater. Interfaces 3 (2011) 4165–4168.
[29] V. Sivasankaran, C. Marino, M. Chamas, P. Soudan, D. Guyomard, J.C. Jumas, P.E. Lippens, L. Monconduit, B. Lestriez, J. Mater. Chem. 21 (2011) 5076–5082.
[30] H.A. Wilhelm, C. Marino, A. Darwiche, L. Monconduit, B. Lestriez, Electrochem. Commun. 24 (2012) 89–92.
[31] D.A. Shirley, Phys. Rev. B 5 (1972) 4709–4714.

[32] J.H. Scofield, J. Electron Spectrosc. Relat. Phenom. 8 (1976) 129.
[33] L. El Ouatani, R. Dedryvère, J.B. Ledeuil, C. Siret, P. Biensan, J. Desbriéres, D. Gonbeau, J. Power Sources 189 (2009) 72–80.
[34] L. Bodenes, R. Naturel, H. Martinez, R. Dedryvèe, M. Menetrier, L. Croguennec, J.-P. Pérès, C. Tessier, F. Fischer, J. Power Sources 236 (2013) 265–275.
[35] J. Vetter, P. Novàk, M.R. Wagner, C. Veit, K.C. Möller, J.O. Besenhard, M. Winter, M. Wohlfahrt-Mehrens, C. Vogler, A. Hammouche, J. Power Sources 147 (2005) 269–281.
[36] D. Aurbach, B. Markovsky, A. Shechter, Y. Ein-Eli, H. Cohen, J. Electrochem. Soc. 143 (1996) 3809–3820.
[37] S. Leroy, H. Martinez, R. Dedryvère, D. Lemordant, D. Gonbeau, Appl. Surf. Sci. 253 (2007) 4895–4905.
[38] R. Dedryvère, L. Gireaud, S. Grugeon, S. Laruelle, J.M. Tarascon, D. Gonbeau, J. Phys. Chem. B 109 (2005) 15868–15875.
[39] S. Leroy, F. Blanchard, R. Dedryvère, H. Martinez, B. Carré, D. Lemordant, D. Gonbeau, Surf. Interface Anal. 37 (2005) 773–781.
[40] L. Baggetto, P. Ganesh, C.-N. Sun, R.A. Meisner, T.A. Zawodzinski, G.M. Veith, J. Mater. Chem. A 1 (2013) 7985–7994.
[41] M. Moshkovich, Y. Gofer, D. Aurbach, J. Electrochem. Soc. 148 (2001) E155–E167.
[42] J.S. Bridel, T. Azaïs, M. Morcrette, J.M. Tarascon, D. Larcher, J. Electrochem. Soc. 158 (2011) A750–A759.
[43] B. Key, R. Bhattacharyya, M. Morcrette, V. Seznéc, J.-M. Tarascon, C.P. Grey, J. Am. Chem. Soc. 131 (2009) 9239–9249.